

Electrochemical exfoliation of graphite in nanofibrillated kenaf cellulose (NFC)/surfactant mixture for the development of conductive paper

Tretya Ardyani^a, Azmi Mohamed^{a,b,*}, Suriani Abu Bakar^b, Masanobu Sagisaka^c, Yasushi Umetsu^c, Mohamad Hafiz Mamat^d, Mohd Khairul Ahmad^e, H.P.S. Abdul Khalil^f, Stephen M. King^g, Sarah E. Rogers^g, Julian Eastoe^h

^a Department of Chemistry, Faculty of Science and Mathematics, Universiti Pendidikan Sultan Idris, 35900, Tanjong Malim, Perak, Malaysia

^b Nanotechnology Research Centre, Faculty of Science and Mathematics, Universiti Pendidikan Sultan Idris, 35900, Tanjong Malim, Perak, Malaysia

^c Department of Frontier Materials Chemistry, Graduate School of Science and Technology, Hirosaki University, Bunkyo-cho 3, Hirosaki, Aomori, 036-8561, Japan

^d NANO-ElecTronic Centre (NET), Faculty of Electrical Engineering, Universiti Teknologi MARA, 40450, Shah Alam, Selangor, Malaysia

^e Microelectronic and Nanotechnology – Shamsuddin Research Centre (MiNT-SRC), Faculty of Electrical and Electronic Engineering, Universiti Tun Hussein Onn Malaysia, 86400, Parit Raja, Batu Pahat, Johor, Malaysia

^f School of Industrial Technology, Universiti Sains Malaysia, 11700, Gelugor, Penang, Malaysia

^g ISIS Pulsed Neutron & Muon Source, STFC Rutherford Appleton Laboratory, Harwell Campus, Didcot, Oxfordshire, OX11 0QT, United Kingdom

^h School of Chemistry, University of Bristol, Cantock's Close, Bristol, BS8 1TS, United Kingdom

ARTICLE INFO

Keywords:

Ionic surfactant
Reduced graphene oxide
Electrochemical exfoliation
Conductive paper
Nanocellulose

ABSTRACT

The effect of incorporating common dodecyl anionic and cationic surfactants such as dodecyltrimethylammonium bromide (DTAB), dodecylethyldimethylammonium bromide (DDAB), and sodium dodecylsulfate (SDS) in nanocomposites of reduced graphene oxide and nanocellulose are described. The stabilization and electrical properties of the nanocomposites of reduced graphene oxide (RGO) and nanofibrillated kenaf cellulose (NFC) were characterized using four-point probe electrical conductivity measurements. Raman spectroscopy, field emission scanning electron microscopy, and high-resolution transmission electron microscopy were used to investigate dispersion morphology and the quality of RGO inside the NFC matrices. Small-angle neutron scattering (SANS) was used to study the aggregation behavior of the aqueous surfactant systems and RGO dispersions. The cationic surfactant DTAB proved to be the best choice for stabilization of RGO in NFC, giving enhanced electrical conductivity five orders of magnitude higher than the neat NFC. The results highlight the effects of hydrophilic surfactant moieties on the structure, stability and properties of RGO/NFC composites.

1. Introduction

There is a strong drive for using nanocellulose in the development of polymer nanocomposites as this offers various benefits including low environmental impact. Recently researchers have been attempting to incorporate graphene into nanocellulose matrices for applications requiring good electrical properties, such as conducting papers (Hou, Xu, & Li, 2018; Wang, Bian, Ji, & Yang, 2018). The most common approach to fabricate graphene/nanocellulose paper is by blending, where the electrical conductivity of the resulting composite is highly dependent on the amount of incorporated graphene and the dispersion quality (Nguyen Dang & Seppälä, 2015; Peng, Meng, Niu, & Lu, 2012; Wang, Drzal, Qin, & Huang, 2015). Numerous studies on graphene/nanocellulose papers have reported remarkable electrical conductivities.

Wang et al. reported a conductivity of $1.98 \times 10^{-1} \text{ S cm}^{-1}$ with a graphene content of 20 wt% (Wang et al., 2018). Previously, Ye et al. (2016) also noted similar conductivities ($1.50 \times 10^{-1} \text{ S cm}^{-1}$), albeit with a higher graphene content (50 wt%). And Xiong et al. (2016) claimed to have reached an electrical conductivity of nearly 50 S cm^{-1} with nanocellulose/graphene oxide nanomembranes at 56.8 wt% graphene content.

One of the merits of nanocomposites reinforced by graphene is the possibility of reaching high and stable electrical conductivities. Problems arise however, because of the difficulty of dispersing graphene in nanocellulose. Furthermore, improving the dispersibility of nanocellulose in aqueous phases is also particularly challenging. Although the aforementioned studies have reported highly conductive graphene/nanocellulose papers, high filler loadings were required,

* Corresponding author at: Department of Chemistry, Faculty of Science and Mathematics, Universiti Pendidikan Sultan Idris, 35900, Tanjong Malim, Perak, Malaysia.

E-mail address: azmi.mohamed@fsmst.upsi.edu.my (A. Mohamed).

<https://doi.org/10.1016/j.carbpol.2019.115376>

Received 24 May 2019; Received in revised form 23 September 2019; Accepted 23 September 2019

Available online 24 September 2019

0144-8617/© 2019 Elsevier Ltd. All rights reserved.

having negative economic and environmental impacts. In most cases, surface modifications are required, or added electrolytes or alkaline conditions are necessary to achieve stable nanocellulose systems (Zhang, Liu, Zheng, & Zhu, 2012; Zhou & Zhang, 2000). Functionalization of graphene is another commonly used method to overcome the challenges of stabilizing dispersions (Georgakilas et al., 2012). Although nanocellulose itself is considered an environmentally safe material, chemical functionalization can compromise this advantage. On the other hand, chemical functionalization of graphene can be expected to affect the π -conjugated network responsible for distributing electrical flow (Mohamed et al., 2016). Therefore, in an effort to seek an economical and effective approach, the focus here is on the use of added surfactants to help improve compatibility between graphene and nanocellulose.

As such, surfactants can be considered an appealing alternative and numerous articles have discussed this approach for enhancing the surface properties of graphene and carbon nanotubes (Mohamed et al., 2016; Tkalya, Ghislandi, de With, & Koning, 2012). We reasoned the same concept could be useful for nanocellulose-graphene composites. Our previous work introduced a simple method for obtaining stable graphene/nanocellulose dispersions with the help of ionic liquid type surfactants (Mohamed, Ardyani, Abu Bakar, Sagisaka, Umetsu & Hussin, 2018). The resulting dispersions could be further cast to generate graphene/nanocellulose conductive papers. Applying similar concepts, and to explore surfactants that are compatible with both graphenes and nanocellulose, the focus here is shifted to cationic surfactants. Since the first report of surfactants for graphene processing emerged, various types have been tested (Lin et al., 2016; Mohamed et al., 2016; Tkalya et al., 2012). Most studies have used anionic surfactants, whereas works with cationic surfactants are more limited. In one early example, a range of quaternary ammonium cationic surfactants were used to prepare surfactant-intercalated graphite oxide (Matsuo, Niwa, & Sugie, 1999). They reported an ability to control interlayer spacing by changing the surfactant type and concentration. Fourier transform infrared (FTIR) spectroscopy results suggested intermolecular interactions between the surfactants and the oxygens of graphite oxide. Later, others demonstrated successful exfoliation of graphite assisted by cetyltrimethylammonium bromide (CTAB) to yield few-layered graphene sheets (Vadukumpully, Paul, & Valiyaveetil, 2009). In a different study, this surfactant was observed to increase the dispersion quality of reduced graphene oxide (RGO) in natural rubber latex (NRL) matrices through conventional mixing. Enhancements of several properties were claimed, although the electrical conductivity was only moderately improved (Matos, Galembeck, & Zarbin, 2014).

Regarding studies with nanocellulose, the majority of surfactants studied are anionic and nonionic (Tardy et al., 2017). A comprehensive understanding of how cationic surfactants affect physicochemical properties would, therefore, underpin the knowledge of the structure–performance relationships of ionic surfactants in these materials. To date, save for a few limited examples (Tardy et al., 2017), literature reports of systematic studies comparing anionic and cationic surfactants in composites of graphene and nanocellulose still remain scarce. This current study investigates how interfacial interactions, system stabilization and physicochemical properties are influenced by the choice of surfactant. Two different cationic surfactants are investigated here, both bearing C12 hydrophobic chains (Table 1): dodecyltrimethylammonium bromide (DTAB) and dodecylethyldimethylammonium bromide (DDAB). From the quaternary ammonium series, DDAB would be the most appropriate to benchmark the performance of DTAB as these surfactants only differ by substitution of a methyl group on DTAB with a longer ethyl chain on the polar head. To provide a comparable alternative, the C12 chain anionic sodium dodecylsulfate (SDS) is also included in the study. The results help to identify efficient commercially available cationic and ionic surfactants for nanocellulose-graphene composites.

2. Materials and methods

2.1. Materials

Dodecyltrimethylammonium bromide (DTAB) and Dodecylethyldimethylammonium bromide (DDAB) were purchased from Acros Organics and used without further purification. Sodium dodecylsulfate (SDS; System) was used as received. Nanofibrillated kenaf cellulose was a gift from the Forest Research Institute Malaysia. Graphite rods with diameter of 10 mm and length of 150 mm were obtained from Goodfellow, GmbH. Hydrazine hydrate was obtained from Merck and used as received. Deuterium oxide (D_2O) was purchased from Apollo Scientific and used as received.

2.2. Preparation of graphene/nanofibrillated kenaf cellulose (NFC) conductive paper (GCP)

2.5 g of NFC was first dispersed in surfactant solutions (0.500, 0.200, 0.100, 0.075 and 0.050 M) to obtain 50 mL NFC/surfactant dispersions. The mixtures were then vigorously stirred for 2 h to form stable dispersions. The surfactant/NFC dispersions were then used as electrolyte for the exfoliation of graphene at a constant voltage of 7 V (GW INSTEK GPS 303000) with graphite rods as both electrodes. The electrochemical exfoliation was carried out at room temperature for 24 h. Next the dispersions were subjected to mechanical stirring and sonication for 1 h, resulting in homogeneous mixtures of graphene oxide (GO)/NFC/surfactant. For the reduction of graphene hydrazine hydrate (0.1 mL hydrazine /10 mL GO dispersion) was used and the reaction was carried out under reflux at 90–100 °C for 24 h. After the reaction was completed, the mixture was then filtered and dried overnight on a filter paper in an oven at 50 °C. Dark to light grey papers (GCP) were obtained by peeling the papers from filter paper substrates. The amount of nanofiller in the GCPs is given in Table S1.

2.3. Preparation of NFC/surfactant composites

The NFC/surfactant dispersions (50 mL) were obtained by dispersing 2.5 g of NFC in surfactant solutions with vigorous stirring for 2 h to form stable dispersions. The mixtures were then filtered and dried overnight on a filter paper in an oven at 50 °C. Similar to the GCP, the NFC/surfactant composites were obtained after peeling the resulting papers off the filter paper substrates.

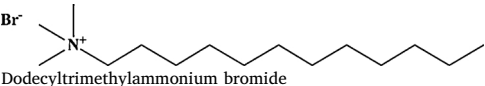
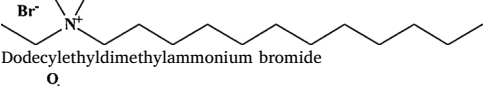
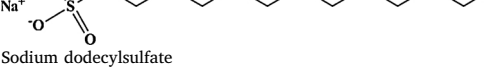
2.4. GCP characterization

The electrical conductivities of the GCPs were measured by a four-point probe method (Keithley 2636A). The morphologies and microstructure of GCPs were observed under a field emission electron microscope (FESEM, Hitachi SU8020). Raman spectroscopy was carried out using a Renishaw InVia micro Raman system spectrophotometer with a 514 nm argon-ion laser source. To visualize the embedded microstructures of nanocellulose papers, high resolution transmission electron microscopy (HRTEM JEOL 2100 F) was used. Prior to HRTEM imaging, the GCPs were cryo-ultramicrotomed with a diamond knife to give sections with nominal thickness ~ 80 nm.

2.5. Zeta potential measurements

Zeta potential measurements were performed using a ELSZ-1000 Zeta-potential and Particle Size Analyzer (Photal Otsuka Electronics) employing the Smoluchowski equation and single peak Lorentz fitting. Measurements were carried out with a flow cell at a sampling time of 400 μ s, cumulative number 7, measuring angle 15°, temperature 25 °C, pin hole size 50 μ m, and cell constant 70.000 cm^{-1} . The properties of aqueous mixtures including refractive index of 1.3328, viscosity of 0.8878 cP, and dielectric constant of 78.3 were used for calculation of

Table 1
Chemical structures of surfactants used in this study.

Abbreviation	Chemical structure and name
DTAB	 <p>Dodecyltrimethylammonium bromide</p>
DDAB	 <p>Dodecylethyldimethylammonium bromide</p>
SDS	 <p>Sodium dodecylsulfate</p>

zeta potential. Zeta potential values were finally obtained as average values of 10 runs for each mixture.

2.6. Small-angle neutron scattering (SANS)

Small-angle neutron scattering (SANS) studies were carried out on the time-of-flight diffractometer LOQ at the ISIS Pulsed Neutron & Muon Source, UK. The accessible Q range was $0.007 - 0.23 \text{ \AA}^{-1}$, arising from incident neutron wavelengths of $\lambda = 2.2 - 10 \text{ \AA}$ at 25 Hz. The SANS samples were prepared in deuterium oxide (D_2O) to enhance the neutron contrast and improve signal-to-noise and contained in 2 mm path-length quartz cells and held in a thermostatted computer-controlled sample changer at 25°C . Absolute scattering intensities $I(Q)$ (cm^{-1}) were determined to within 5% by measuring the scattering from a partially-deuterated polymer standard of known molecular weight and hence known $I(0)$. The instrument-independent SANS data, reduced using the Mantid framework (www.mantidproject.org), were then model-fit using the SasView program (www.sasview.org) constraining scattering length densities and other known parameters to *a priori* values. Unknown structural parameters were allowed to refine during the fitting process to obtain an optimized fit as required by the different scattering model functions. The SANS data are presented as a function of the (magnitude of) the scattering vector, $Q = (4\pi/\lambda) \sin(\theta)$, where θ is half of the scattering angle. The approximate size of a feature is thus $2\pi/Q$.

3. Results and discussion

3.1. Electrical properties of graphene/NFC paper (GCP)

Greyish paper disks having diameters of 6.50–6.57 cm and 0.14 – 0.18 mm in thickness were obtained. The four-probe electrical conductivities of the papers at room temperature are summarized in Table 2. The relationship between the electrical conductivity achieved by the GCPs and the surfactant concentration is depicted in Fig. S1. As expected, the use of surfactants for improving RGO dispersion inside

the NFC matrices leads to enhancements in electrical properties of NFC paper. Comparisons between samples with and without RGO clearly show that this is due to the presence of RGO dispersed in the NFC matrix.

In general, anionic surfactant SDS brings only moderate improvements in the electrical properties of GCPs, with the highest conductivity achieved at $9.95 \times 10^{-7} \text{ S cm}^{-1}$. Meanwhile, cationic surfactant DTAB improves conductivity by six orders of magnitude, relative to neat NFC, achieving 1.28×10^{-4} at surfactant concentration of 0.200 M. That the electrical conductivities increase with increasing surfactant concentration is a trend reported previously (Mohamed, Ardyani, Abu Bakar, Sagisaka, Umetsu & Hamon, 2018; Suriani, Nurhafizah, Mohamed, Zainol, & Masrom, 2015). Interestingly, however, the effects of surfactants reach a limit, as has also been reported in previous literature (Coleman, 2009; Wang, Yi, & Shen, 2016). The presence of high surfactant concentrations in the nanocomposites was presumed to enhance the electrical conductivity of the nanocomposites (Tkalya, Ghislandi, Alekseev, Koning, & Loos, 2010).

Moving to the measurements of GCP with DDAB surfactant ($1.02 \times 10^{-6} \text{ S cm}^{-1}$), it was found that there is a moderate decrease of the electrical conductivity of the GCPs. The slightly higher carbon number for DDAB (as compared to DTAB) gave a rather limited electrical conductivity enhancement with only four orders magnitude improvement compared to the neat NFC ($1.97 \times 10^{-10} \text{ S cm}^{-1}$). It might be expected that longer surfactant tails (higher C – number) will occupy a larger area on the graphene surfaces (Adamczyk, Para, & Warszyński, 1999; Manne, Cleveland, Gaub, Stucky, & Hansma, 1994; Matsuo et al., 1999; McCoy et al., 2018; Moulik, Haque, Jana, & Das, 1996). Thus, they could provide a greater barrier to water contact at the graphene surfaces, which may lead to destabilization. However, this is not observed in the current study.

In earlier work, Matsuo and co-workers revealed that the interlayer distance of graphite oxide concurrently increases with surfactant alkyl chain length (Matsuo et al., 1999). This may lessen the tendency of adjacent graphene sheets to aggregate. It was presumed that the surfactant forms bilayers between the graphite oxide sheets, where longer

Table 2
Electrical conductivities of NFCs with and without RGO stabilized by surfactants.

Sample	Surfactant concentration (M)				
	0.050	0.075	0.100	0.200	0.500
Electrical conductivity of nanocomposites (S cm^{-1})					
NFC/RGO/DTAB	$3.12 \times 10^{-8} \pm 9.98 \times 10^{-7}$	$1.11 \times 10^{-6} \pm 1.02 \times 10^{-7}$	$2.56 \times 10^{-5} \pm 1.08 \times 10^{-5}$	$1.28 \times 10^{-4} \pm 9.85 \times 10^{-5}$	$5.44 \times 10^{-5} \pm 1.11 \times 10^{-5}$
NFC/RGO/DDAB	$4.46 \times 10^{-8} \pm 8.96 \times 10^{-7}$	$4.76 \times 10^{-8} \pm 2.78 \times 10^{-7}$	$1.43 \times 10^{-7} \pm 1.43 \times 10^{-8}$	$1.02 \times 10^{-6} \pm 8.73 \times 10^{-7}$	$9.75 \times 10^{-7} \pm 1.29 \times 10^{-7}$
NFC/RGO/SDS	$2.82 \times 10^{-8} \pm 8.45 \times 10^{-9}$	$2.08 \times 10^{-8} \pm 7.98 \times 10^{-10}$	$3.09 \times 10^{-7} \pm 2.86 \times 10^{-8}$	$8.92 \times 10^{-7} \pm 1.30 \times 10^{-7}$	$9.95 \times 10^{-7} \pm 6.78 \times 10^{-8}$
NFC	$1.97 \times 10^{-10} \pm 1.59 \times 10^{-9}$				
NFC/DTAB	$1.78 \times 10^{-9} \pm 9.15 \times 10^{-8}$	$5.83 \times 10^{-9} \pm 2.05 \times 10^{-8}$	$9.82 \times 10^{-9} \pm 6.14 \times 10^{-8}$	$5.94 \times 10^{-9} \pm 7.82 \times 10^{-8}$	$1.37 \times 10^{-9} \pm 8.10 \times 10^{-8}$
NFC/DDAB	$3.23 \times 10^{-9} \pm 1.49 \times 10^{-8}$	$3.67 \times 10^{-9} \pm 4.36 \times 10^{-8}$	$7.32 \times 10^{-9} \pm 5.32 \times 10^{-8}$	$7.62 \times 10^{-9} \pm 4.81 \times 10^{-8}$	$7.17 \times 10^{-9} \pm 8.28 \times 10^{-8}$
NFC/SDS	$6.03 \times 10^{-9} \pm 2.04 \times 10^{-8}$	$5.76 \times 10^{-9} \pm 1.01 \times 10^{-8}$	$9.32 \times 10^{-9} \pm 8.24 \times 10^{-8}$	$8.88 \times 10^{-9} \pm 5.21 \times 10^{-8}$	$9.45 \times 10^{-9} \pm 1.24 \times 10^{-9}$

tails (larger areas occupied by surfactant tails) hinder dense packing on the graphite oxide surfaces. Studying dispersions of graphene with ionic surfactants, Smith and co-workers also noted improved dispersion stability using a cationic surfactant with higher C – number (Smith, Lotya, & Coleman, 2010). Although the longer tail achieves a lower dispersion concentration, it provides greater stability, after 7 days of observation. This idea is again inconsistent with the trend reported here.

Looking at the electrical conductivity of GCPs over all surfactant concentrations, DTAB maintains higher conductivity compared to SDS and DDAB. It therefore can be suggested that the stability of GCP suspensions are sensitive to the chemical structure of the hydrophilic moieties of the stabilizing surfactants. That result would be in agreement with Quennouz and co-workers who also highlighted the effect of surfactant hydrophilic structure on the stability of surfactant/cellulose nanofibril suspensions, where SDS required a 20-fold higher concentration than DTAB to give the same suspension stability (Quennouz, Hashmi, Choi, Kim, & Osuji, 2016). This phenomenon can also be explained from the viewpoint of RGO and surfactant affinity. McCoy et al. (2018) revealed that the headgroup type is the overriding factor for affinity between surfactants and RGO surfaces, as cationic surfactants proved to be more attractive for RGO surfaces than anionics.

Looking at the conductivity values of the GCPs, the results obtained here are over a similar range to those reported in other related studies (see Table S2) (Feng, Zhang, Shen, Yoshino, & Feng, 2012; Kiziltas et al., 2016; Wang et al., 2015). Rather than obtaining high conductivity values with a high amount of nanofiller (Wang et al., 2018; Ye et al., 2016), here it is shown that an improvement in the NFC nanocomposite electrical properties can be expected at considerably lower nanofiller contents (see Table S1 and S2) with the help of surfactant. Overall, the cationic DTAB provided significantly higher conductivity enhancement compared to cationic DDAB and anionic SDS. In these systems, when using surfactants with the same alkyl chain length, it seems that cationic surfactants are the best choice for optimizing the resulting nanocomposite properties.

3.2. Raman spectroscopy of graphite and graphene/NFC paper (GCP)

Raman spectroscopy was used to analyze the structural changes experienced by the starting material graphite into reduced graphene oxide contained in GCPs. The prominent peaks of graphene based materials located at 1350 (D-peak) and 1580 cm^{-1} (G-peak) (Ferrari, 2007) are displayed in Fig. 1. The peak positions of each sample are summarized in Table S3 (Supplementary material). Graphite has a

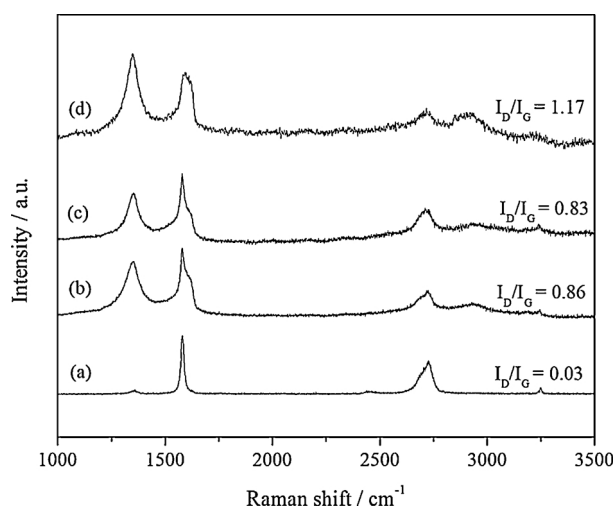


Fig. 1. Raman spectra of the graphite (a) and GCPs stabilized with cationic surfactants: (b) DTAB, (c) DDAB and anionic surfactant: (d) SDS. Surfactant concentration: 0.100 M.

negligibly small and weak D-peak. The G-peak located at 1581 cm^{-1} is clearly more intense than the D-peak. As the graphite was exfoliated, oxidized, and subjected to chemical treatment (reduction process to restore the sp^2 -conjugated network) to transform into a reduced graphene oxide, the D and G peak evolve significantly. In the GCPs samples, the D-peak is clearly identifiable with prominent peaks. At the higher wavenumber side (2D area; 2700 cm^{-1}), it can be seen that graphite displayed a single broad peak, while the GCPs have slimmer and less sharp peaks with a bump like region. The existence of the bump like areas might be due to the presence of chemically induced defects during the GCP fabrication process (Kaniyoor & Ramaprabhu, 2012).

As a consequence of the oxidation and reduction process, the defects increase, leading to an increase in the D-peak intensity (I_D). To characterize the lattice structure of RGO, the ratio of Raman intensities (defect to graphitic ratio; I_D/I_G) was calculated, where lower I_D/I_G indicates lower defects in the graphene structure. As can be seen, the I_D/I_G ratio of graphene presented in the GCP significantly increased compared to the starting material (graphite), implying that the exfoliation and reduction process has been successful (Chua & Pumera, 2013; Kudin et al., 2008). Comparison of I_D/I_G values between the GCPs shows that the sample with SDS gives the highest Raman ratio. The results suggest that RGO in GCPs stabilized by SDS has the highest level of remnant functional groups, and the sp^2 -carbon basal plane is less healed during the reduction process compared to DTAB or DDAB. Correlating the I_D/I_G ratio with electrical properties of the GCPs reveals a pattern of higher conductivity for GCP with lower defect ratios. Here, the choice of surfactant can be linked with the quality of RGO produced during the fabrication process, whereby better surfactants produce RGO with lower defect densities, and thus higher electrical conductivities. Although such trends are noted, it can be seen that the I_D/I_G difference between DTAB and DDAB is close. Hence, more detail is necessary to evaluate those factors affecting the different performance of surfactants in this series, particularly between DTAB and DDAB.

3.3. Morphology of graphene/NFC paper (GCP)

The internal structure of RGO dispersions inside NFC matrices was investigated by FESEM. Fig. 2 shows FESEM images of the GCPs as well as the NFC. As shown in Fig. 2a, NFC exhibits a random arrangement of tapelike fibrils having a diameter of 32–49 nm without any preferential orientation. In the case of the GCPs (Fig. 2b–d), various morphologies of nanofiller can be seen decorating the NFC fibers. Different regions of NFC fibrillated networks can be seen, and RGO can be identified as aggregates (Fig. 2c and d) or more defined stacked layered structures (Fig. 2b).

Comparison of the GCP morphologies with different surfactants at low magnification (Fig. 2b–d) reveal that RGOs produced using DTAB and DDAB have considerably larger sizes compared with SDS. GCPs stabilized with DTAB appear to feature large flaked RGO regions, although, closer observation (Fig. 2b') reveals less defined sheets edges with a stacked structure. Meanwhile, RGO in GCPs with DDAB (Fig. 2c and c') and SDS (Fig. 2d and d') exist as aggregated structures under both high and low magnification imaging, unlike those observed with DTAB. Based on the FESEM results, it is considered that the RGO can be successfully dispersed into the NFC matrices. The observations also tie in well with the trends in electrical conductivity discussed above.

It is known that the electrical conductivity of a nanocomposite is affected by the dispersion state of the nanofiller inside the host. In this case, more uniformly distributed nanofillers are expected to give higher electrical conductivities (Mao, Zhu, & Jiang, 2012; Tkalya et al., 2012). In addition to this, the electrical properties also depend on the quality of the graphene where more exfoliated graphene sheets lead to higher electrical conductivity (Mao et al., 2012). Visualization of the RGOs inside NFC matrices using FESEM revealed different morphologies resulting from different surfactants. From these images it can be deduced that DTAB offers better exfoliation and stabilization than SDS and

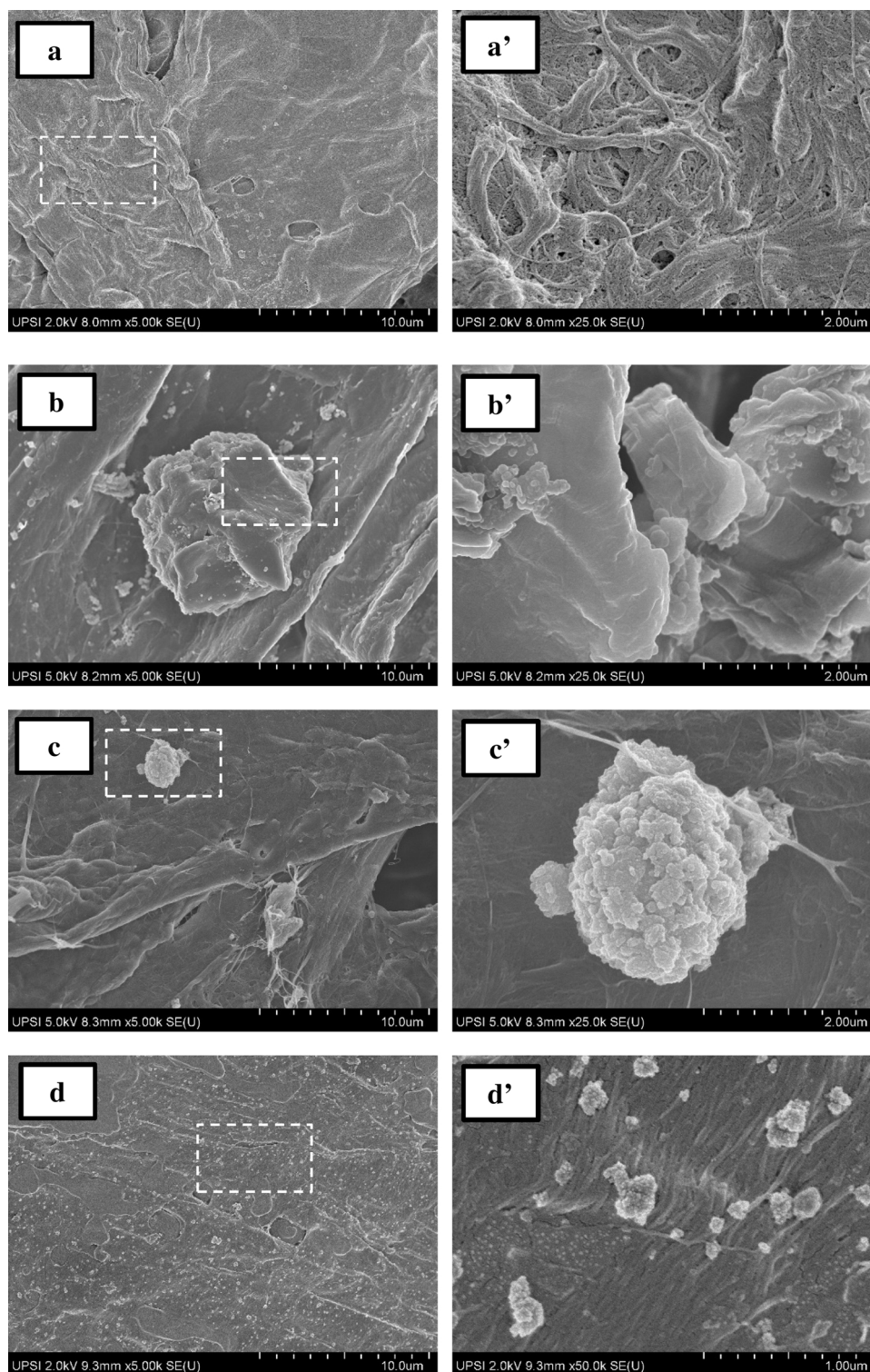


Fig. 2. FESEM images of nanofibrillated kenaf cellulose (NFC) (a and a') and GCP: with DTAB (b and b'), with DDAB (c and c'), and with SDS (d and d'). The selected areas for higher magnification imaging are marked by the dashed squares.

DDAB, yielding defined flakes rather than aggregated structures.

The results and trends obtained here agreed well with the electrical conductivity measurements described above. However, linking the morphology of the RGOs inside the GCPs does not lead to such obvious trends as for the electrical conductivity measurements. But, on the whole, by comparing the morphology of the GCPs it is reasonable to conclude that DTAB is the best dispersant out of the surfactants used in this study.

The FESEM images have highlighted the different RGO morphologies dispersed in NFC matrices. In order to understand the embedded microstructure of RGO inside NFC stabilized by DTAB surfactant, an ultrathin section of RGO was observed under HRTEM. Observations at low magnification (Fig. 3(a and b) indicate the presence of RGO (dark lines), supporting the FESEM images. An enlarged view (Fig. 3c) revealed that RGO was present as few-layer sheets. Hence, it is seen that DTAB is a good surfactant for this application.

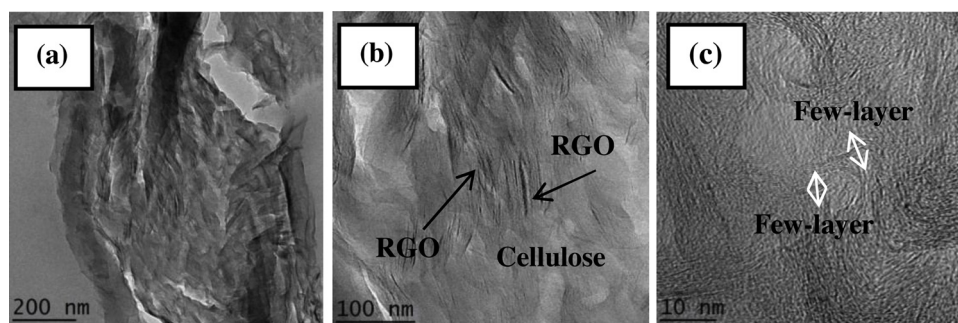


Fig. 3. HRTEM images of the GCP stabilized by DTAB: (a) Typical morphologies at low magnification (b) higher magnification. Grey areas are NFC fibers. Note that many RGO sheets are embedded throughout the NFC matrix (c) Edge view of RGO sheets.

3.4. Studying the role of surfactant for dispersion stability: Zeta (ζ)-potential measurements

In aqueous dispersions, the electrical double layer is an important feature and zeta potential measurements are a useful means to assess colloidal stability (Hunter, 1981). The addition of electrolytes may affect the distribution of surface charge, depending on the nature of the added component. Efforts to make a comparison with literature values, however, are restricted due to the very limited number of studies focused on the colloidal stability of these types of systems.

To provide understanding of the surfactant stabilization process and its relationship, if any, to the efficiencies in elevating the composite properties, the zeta potentials of RGO dispersions stabilized by DTAB, DDAB, and SDS were measured. The values are given in Table 3. The RGO dispersion quality and the ability of surfactant to impart stabilization scales very well with the measured zeta potentials. The sign of the zeta potential (negative or positive) reflects the type of surfactant adsorbed onto the material. As a rule of thumb, systems with a zeta potential of $[10 - 20]$ mV is close to the threshold of agglomeration whereas a value of $[30]$ mV or higher is accepted as necessary for colloidal stability (Lotya et al., 2009).

Between the cationic surfactants, although DTAB displayed a zeta potential above that needed for a stable colloidal system, $+32$ mV, its cousin DDAB exhibited a zeta potential of $+23$ mV, very close to the stability boundary. In contrast to the results obtained here, Smith et al. noted very good graphene dispersion stability using quaternary ammonium bromide surfactants (zeta potential $> +45$ mV) (Smith et al., 2010). Interestingly, SDS outperforms both DTAB and DDAB in terms of zeta potential, exhibiting a value of -43 mV.

Simply on the basis of the results from the zeta potential measurements, SDS should offer significantly more stability than DTAB and DDAB, and so SDS should confer better electrical properties on the nanocomposites than either cationic surfactant. The results from the electrical conductivity measurements in Table 2, however, did not follow this order. This suggests there must be another factor responsible for attenuating the reinforcing factor of RGO with SDS. Intermolecular

interactions between each component: RGO, surfactants, and NFC, therefore need to further investigation to explain this behavior. And these observations may facilitate a rationale for selecting more suitable surfactant types for the development of conductive papers of nanocellulose and graphene.

3.5. Effect of headgroup type on surfactant aggregation structure: small-angle neutron scattering (SANS) study of surfactant solutions and reduced graphene oxide (RGO)-stabilized surfactant systems

Surfactants will self-assemble into micelles in the aqueous phase driven by the tendency of hydrophobic tails to minimize contact with water. When carbon nanomaterials are also present, surfactants can adsorb at the solid-liquid interface in various configurations (Lin et al., 2016; Tkalya et al., 2012; Vaisman, Wagner, & Marom, 2006). Thus, it is important to understand the interfacial organization of the surfactants on RGO surfaces, and for this small-angle neutron scattering (SANS) studies have been conducted. SANS studies can give quantitative information about the shape and size of the surfactant aggregation structures in aqueous phases and in RGO dispersions. Such information will contribute to a better understanding of the interactions between RGO and the surfactants, as well as provide insights into the structure and nature of the adsorbed surfactant layers.

Fig. 4 shows SANS data for the surfactant solutions and RGO dispersions with DTAB, DDAB, and SDS. The scattering intensity $I(Q)$ is related to the nanostructure present: the features contributing to $I(Q)$ are the shape and size of the particles, usually described as a particle form factor $P(Q)$, the dispersion concentration, and the scattering contrast of the particles relative to the dispersion medium. With charged particle dispersions, the scattering profile is also affected by inter-particle interactions which can be either attractive or repulsive in nature. These are accounted for by the structure factor $S(Q)$. For more detailed discussions on SANS, readers are directed elsewhere (Feigin & Svergun, 1987; Hollamby, 2013).

For SDS, the scattering profile agrees well with a model for charged spherical micelles, consistent with the literature (Paul et al., 2005; Yurekli, Mitchell, & Krishnamoorti, 2004). The interparticle interaction was fitted to a Hayter-Penfold Mean Spherical Approximation $S(Q)$ model (Hayter & Penfold, 1983), with the fit parameters listed in Table S4. The model-fitting returned a micellar radius R_{sphere} of 22.0 Å (see Table 3), consistent with previous works (Magid, Li, & Butler, 2000; Mohamed, Ardyani, Abu Bakar, Sagisaka, Umetsu, Hussin et al., 2018; Wang et al., 2016; Yurekli et al., 2004), and acts as an important validation of the methods used here.

In contrast, measurements with the cationic surfactant DTAB gave $I(Q)$ data characteristic of ellipsoidal micelles experiencing repulsive interactions, which again were modelled by the Hayter-Penfold $S(Q)$. An axial micelle radius, R_a , of 15.0 Å (Table 3) was obtained with an aspect ratio, X , 1.5 indicating that the micelles are oblate spherical ($R_a < R_b$). This result is also consistent with literature values which report axial radii between 15.0 – 19.0 Å at surfactant concentrations of

Table 3
Model fit parameters for SANS data.^a

Sample	ζ -potential (mV)	Model	R_{sphere} (Å)	R_a (Å)	$X \pm 0.2$
DTAB	–	Ellipsoid	–	15.0	1.5
DDAB	–	Ellipsoid	–	11.0	2.2
SDS	–	Sphere	22.0	–	–
DTAB + RGO	$+32 \pm 1$	Ellipsoid	–	14.0	1.7
DDAB + RGO	$+23 \pm 1$	Sphere	17.0	–	–
SDS + RGO	-43 ± 4	Sphere	24.0	–	–

^a [surf.] = 0.030 M. Charged micelles were fitted by incorporating the Hayter-Penfold Mean-Spherical Approximation interparticle structure factor. X is the aspect ratio.

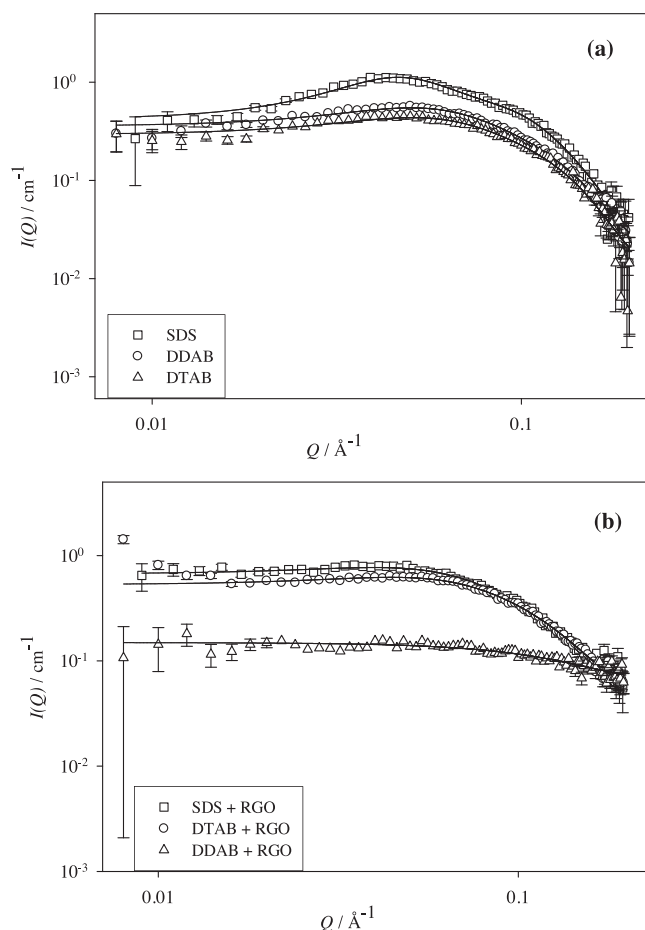


Fig. 4. SANS profiles for (a) DTAB, DDAB, and SDS solutions and (b) the RGO dispersions in D_2O . [surfactant] = 0.030 M and $T = 25^\circ C$. Lines are model fits for charged homogeneous spherical or ellipsoidal micellar $P(Q)$ with a Hayter-Penfold Mean-Spherical Approximation $S(Q)$. Characteristic error bars are shown for the lowest intensity samples.

0.02 – 0.20 M (Brown et al., 2012; Griffith & Notley, 2012; Mahajan, Vohra, Kaur, & Aswal, 2008; McCoy et al., 2018). Bergström and Pedersen (1998, 1999) also investigated the self-assembly of ellipsoidal micelles, although in their study, the form factor $P(Q)$ used was a triaxial ellipsoidal model.

The scattering data from the DDAB surfactant is also described by an ellipsoidal form factor, again with a broad peak from the electrostatic interparticle stabilization of the micelles. Fitting these SANS data gave an axial radius of 11.0 Å with an aspect ratio of 2.2. It seems that the secondary axis of DDAB micelles is larger than for DTAB micelles at the same concentration. This increase in micellar radius can be attributed to the increased length of the surfactant tail. Previous SANS experiments on cationic ammonium halide surfactants revealed an increase of micellar radii with longer hydrophobic tails (Aswal & Goyal, 1998; Berr, 1987; McCoy et al., 2018).

Parallel SANS experiments were then conducted at the same surfactant concentration but with RGO incorporated, and the results compared to those for the pure surfactant solutions in order to reveal any structural changes. In doing so we exploited a key feature of SANS: that a component of a mixture with a very similar scattering length density to the dispersion medium has no neutron contrast and so is effectively invisible (or ‘contrast-matched’ in the vocabulary of SANS). No substantial difference in scattering between these RGO-containing samples and the pure surfactant solutions was observed over the Q range studied, and the SANS data can again be adequately fitted with the ellipsoidal and spherical models as appropriate. As can be seen in

Table 3, the micellar dimensions are broadly the same for DTAB and SDS. This is surprising for DTAB, as it is the most efficient surfactant in the series. A micelle shape transition, or changes in dimensions, are to be expected when such low dimensional material is added to the system, as those found in the existing literature (Granite, Radulescu, & Cohen, 2012; McCoy et al., 2018; Wang et al., 2004). McCoy et al. found significant differences in the scattering profile in the low Q region ($0.003 - 0.02 \text{ Å}^{-1}$), following the Q^{-2} indicative of planar flat RGO sheets, which was not found in this study (McCoy et al., 2018). In contrast, DDAB transitioned into a different micellar shape: an ellipsoidal to spherical transition was observed. If only considering the axial radius of ellipsoids, the presence of RGO resulted in a larger micellar radius 17.0 Å.

Comparison of the scattering profiles between Fig. 4a and b give evidence of the changes on the intermicellar interaction when RGO is added in surfactant solutions. The $S(Q)$ peak (or the appearance of “bump” in the scattering profile) in Fig. 4b is less pronounced, suggesting fewer intermicellar interaction (Hayter & Penfold, 1983). We may note that this is because adding RGO has neutralized some of the charges. As can be seen in Table S4 the micellar charge z as defined in the Hayter-Penfold structure factor seems to decrease about 4.00–8.00 when RGO is introduced in the system. In general, although analysis of the SANS data revealed physically realistic parameters, it is rather challenging to draw a firm trend or pattern about the self-assembly of the surfactants on RGO surfaces from it.

The existing literature suggests certain arrangements of surfactant molecules on graphene surfaces as a characteristic of positive surfactant – graphene interactions, for example hemi-micelles, or cylindrical structures (for the case of CNTs) (Lin, Shih, Strano, & Blankschtein, 2011, 2016; Matarredona et al., 2003). With this picture in mind, it can be suggested that the adsorption of surfactant on graphene surface is low due to the less favorable interactions of dodecyl tails and graphene surfaces. Hence most surfactant molecules are still in the bulk micelle. The surfactants are presumed to just randomly adsorb on graphene surface, enough to prevent the adjacent neighboring RGO sheets from aggregating and destabilizing.

3.6. Comparison of cationic vs. anionic surfactants at graphene and NFC interfaces: a proposed mechanism

A significant advancement in studying the adsorption of surfactant at carbon nanomaterial surfaces has been the use of small-angle neutron scattering and molecular dynamic simulations (Lin et al., 2011; McCoy et al., 2018; Wang, 2009). With these techniques, insight into how the surfactant adsorbs can be postulated. In this study, the cationic DTAB was identified as the most efficient for stabilizing the RGO/NFC composites in terms of its zeta potential. However, the SANS data do not show any structural changes of the DTAB micelles. Despite giving a higher conductivity enhancement, DTAB still behaves in a similar fashion to anionic SDS and cationic DDAB.

There is strong evidence of the relationship between stability and the tendency of surfactants to follow the curvature of dispersed materials (Matarredona et al., 2003; Vaisman et al., 2006; Wang et al., 2004; Wang, 2009). However, this is not the case here; therefore, a model of fully-surfactant covered graphene surfaces as has been used to explain aggregation behavior in a previous study (Mohamed, Ardyani, Abu Bakar, Sagisaka, Umetsu, Hussin et al., 2018; Mohamed, Ardyani, Abu Bakar, Sagisaka, Umetsu, Hamon et al., 2018) must be ruled out here too.

In an earlier study, Yurekli et al. (2004) assumed a structureless random adsorption of SDS on single walled carbon nanotube (SWCNT) walls being responsible for the aqueous phase dispersion stability. This stems from the constant micelle shape and size upon SWCNT addition. Instead of adopting cylindrical micelles, SDS molecules were suggested to randomly adsorb at the graphene sheets of CNTs with no preferential arrangement. This picture also is used to explain the behavior of all the

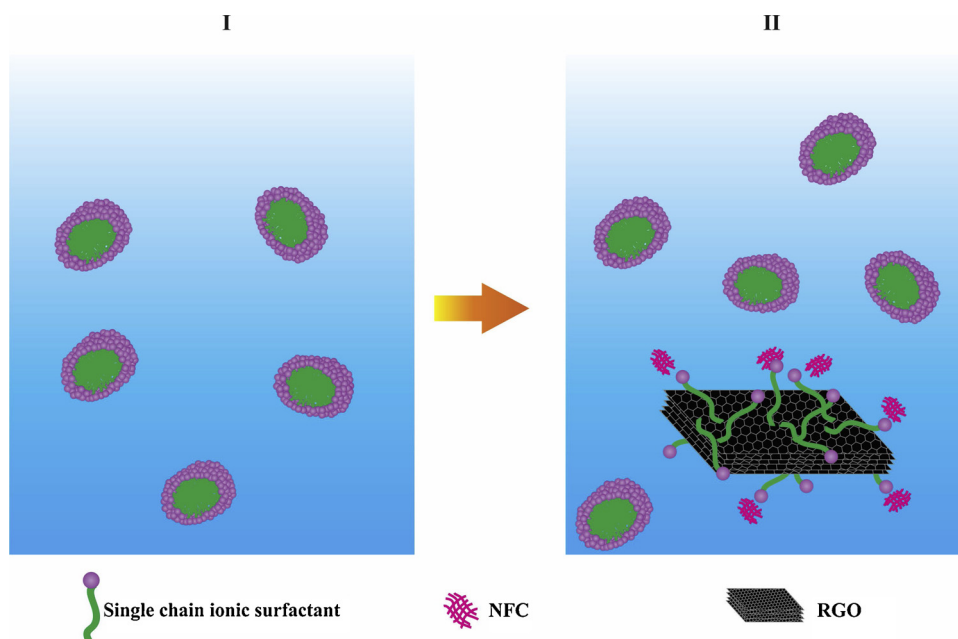


Fig. 5. Proposed mechanism of ionic dodecyl surfactant arrangement in RGO/NFC composites.

surfactants used in this study. A schematic figure of the surfactant self-assembly is given in Fig. 5.

In the stable dispersions surfactant may exist as individual molecules, in micelles, or adsorbed to graphene surfaces (Sa & Kornev, 2011; Wang et al., 2004). The ideal situation would be that the surfactant fully wraps the graphene surfaces, minimizing contact with water, hence adopting the shape of graphene, either as stacked disks or stacked bilayer aggregates. This can be achieved when the attraction between surfactant tails, or headgroups, and the graphene surfaces is strong enough. In this case, the interaction between the surfactants and graphene surfaces may be less favorable, hence the limited number of surfactant monomers adsorbed on graphene surfaces (McCoy et al., 2018; Wang, Han, Wang, Qin, & Guo, 2008).

The surfactant tails are thought to adsorb toward the graphene surfaces by lying flat to maximize the hydrophobic interactions with no preferential adsorption site (Fig. 5 (II)). The charged headgroups are expected to face toward the aqueous phase and interact with the hydrophilic segments of nanocellulose (Bandyopadhyay, Shelley, Tarek, Moore, & Klein, 1998; Ducker & Grant, 1996; Shah, Chiu, & Sinnott, 2006; Wang et al., 2008). If only a limited amount of surfactant is adsorbed on the graphene the surfactant molecules cannot form aggregated structures on the graphene surface and, in turn, the associated surfactant predominates in micelles in the aqueous phase. This may explain the absence of micellar structural transitions in the presence of graphene as observed by SANS.

It has been widely suggested that anionic surfactants are more efficient for stabilizing graphene dispersions (Lin et al., 2016; Shih, Lin, Strano, & Blankschtein, 2015; Smith et al., 2010; Texter, 2014). Notley (2012), however proved otherwise. Using a continuous surfactant addition approach, cationic surfactants (CTAB, DTAB, TTAB) were revealed to be on a par with anionic surfactant (SDS) in terms of the dispersed graphene concentration they produced. In the graphene dispersion literature (Texter, 2014), when the surfactant comprises similar long carbon chains, it is actually very difficult to say which of the stabilizers is better, as different works indicate different conclusions.

It is known that the positioning of surfactants at an interface between water and another phase is a result of an interfacial energy minimization for the surfactant, water and graphene (Coleman, 2009). Therefore, the ability of surfactants to provide stabilization may be assessed through surfactant geometrical considerations, namely

fractional free volume (FFV) (Stone, Smith, da Rocha, Rossky, & Johnston, 2004). This concept was initially introduced to understand the design of effective surfactants for microemulsion studies (Mohamed et al., 2010). As such, it is used to quantify the bulkiness of surfactants at an interface and, hence, the space available for interpenetration between two incompatible materials can be assessed. In polymer science, free volume is important parameter to define the permeability of polymers. Here, the FFV is defined in Eq. (1) as

$$\text{FFV} = 1 - \frac{V}{tA_h} \quad (1)$$

Where, V is the volume of a surfactant tail, t is the thickness of the interface, and A_h is the interfacial area per headgroup. To implement a succinct discussion, the justification made for the FFV calculation as well as the details of each parameter is given in the Supplementary Material (Tables S5 and S6). It is hypothesized here that a lower FFV will minimize the penetration of water at graphene surfaces, hence giving higher conductivity of the GCPs.

As can be seen in Table S7, surfactant performance in stabilizing RGO and NFC dispersions, that is, optimum electrical conductivity, does show a general trend with FFV. In fact, the electrical conductivity increases as FFV decreases. Lower FFV should favor a lower area for water penetration onto the graphene surface and thus promote greater dispersion stability. In support of this interpretation, analysis using fluorescence spectroscopy revealed that the void space near the DTAB headgroup is less than around SDS, suggesting larger water permeability with SDS (Karukstis, Suljak, Waller, Whiles, & Thompson, 1996). Calculation of headgroup surface area through modeling also revealed a larger area occupied by DTAB than by SDS (Karukstis et al., 1996). In general, our results seem to show that the surfactant performance at the graphene – water interface correlates with the FFV.

As well as surfactant structure and architecture, it is also interesting to consider the influence of surfactant activity in stabilizing these composites. A recent review has summarized extensive work on the interaction of cationic and anionic surfactants with nanocellulose (Tucker, Petkov, Penfold, & Thomas, 2012). The nature of surfactant adsorption onto NFC surfaces is broadly similar to other hydrophilic/hydrophobic solid surfaces; except there is an additional aspect to be considered arising from cellulose swelling (Tucker et al., 2012).

By measuring the adsorption isotherm, Biswas and Chattoraj (1997)

proposed that the interaction between homologous ammonium halide surfactants and cellulose involved hydrophobic interactions between the surfactant tails and cellulose surfaces (Biswas & Chatteraj, 1997). Meanwhile, based on the adsorption of CTAB onto anionic nanofibrillated cellulose, others have postulated that the formation of surfactant bilayers effectively makes the cellulose nanofibrils more hydrophilic (Xhanari, Syverud, Chinga-Carrasco, Paso, & Stenius, 2011). The interaction was suggested to be driven by electrostatic interactions between anionic carboxyls present in the nanofibrils with the positively charged CTAB headgroups. Using SDS, Tucker et al. observed the adsorption of surfactant molecules toward the hydrophilic part of negatively charged cellulose at concentrations greater than 2×10^{-3} M (Tucker et al., 2012). Others have proposed the formation of bridging-mediated fibrous networks between SDS and negatively charged nanofibrils (Quennouze et al., 2016). Such networks can be induced by the presence of favorable, albeit weak, interactions between groups in SDS and negatively charged species in cellulose nanofibrils. These studies proved that regardless of the headgroup type, ionic surfactants will be able to display affinity with cellulose surfaces.

Tardy et al. (2017) listed plausible reasons why cationic surfactants outperform anionics for stabilizing these dispersions. The rate of anionic surfactant adsorption at the cellulose-water interface was said to be lower than that of cationic surfactants (Paria, Manohar, & Khilar, 2004). Even when compared to other surfactant types, the kinetics are the fastest and the forces of interaction are the strongest between cellulosic materials and cationic surfactants (Tardy et al., 2017). Studying the rheology of cellulose nanofibrils, Quennouze and co-workers noted that DTAB needed only approximately one eighth of the SDS concentration to form homogeneous clear gel suspensions (Quennouze et al., 2016). The underlying reason for the higher DTAB efficiency, and for cationic surfactants in general, is possibly increased affinities between surfactants and nanocellulose surfaces, facilitating the dispersion of RGO inside NFC matrices.

4. Conclusions

The advantages in utilizing electrochemical approaches to produce dispersed reduced graphene oxide (RGO) have already been established (Parvez et al., 2014; Suriani et al., 2015; Suriani et al., 2016). Our previous study has shown that it is possible to obtain electrically conductive NFC paper stabilized by specialized ionic liquid-type surfactants (Mohamed, Ardyani, Abu Bakar, Sagisaka, Umetsu, Hussin et al., 2018). Here, more common and readily available commercial surfactants are employed instead, and the effects of headgroup chemistry with two model ionic surfactants –anionic and cationic – was investigated in terms of dispersion stability, electrical conductivity enhancement, and aggregation properties. There is a distinct graphene-compatibility order between the anionic and cationic surfactants, with DTAB being the most efficient stabilizer overall. Although the chemical structures of DTAB and DDAB differ only by substitution of a headgroup methyl moiety by an ethyl group, it is still not clear why DDAB does not perform as well as its homologue DTAB. Considering these two analogues have very similar solution properties (Fiscaro, Biemmi, Compari, Duce, & Peroni, 2007), DDAB would be expected to give similar dispersion stability as DTAB.

One way to consider adsorption is in terms of adsorption strength and surface aggregate structures (Mohamed, Ardyani, Abu Bakar, Sagisaka, Umetsu, Hussin et al., 2018; Mohamed, Ardyani, Abu Bakar, Sagisaka, Umetsu, Hamon et al., 2018; Tkalya et al., 2012; Vaisman et al., 2006). The strength and type of interfacial interaction can be expected to influence the morphology of aggregates formed on RGO surfaces. Nevertheless, here a similar micelle structure was seen in both the aqueous solutions and RGO dispersions. The stabilization mechanism was therefore proposed to be random adsorption of surfactant molecules on graphene surfaces, co-existing with surfactant micelles in the bulk. Because the surfactants bear the same C12 hydrophobic tails,

it is reasonable to assume that the any changes in adsorption and stabilization are a result of hydrophilic headgroup structure. A readily calculated empirical surfactant parameter, namely the FFV, is seen to be useful for describing the different behavior between anionic and cationic surfactants. A decrease in FFV favors a more stable system and thus higher electrical conductivity of the composites. The results underline that the choice of surfactant headgroup significantly affects the affinity with RGO and nanocellulose.

Acknowledgements

The work funded under grants from Universiti Pendidikan Sultan Idris Rising Star Research Grant (Grant Code: 2019-0118-103-01). This project was supported by JSPS [KAKENHI, Grant-in-Aid for Young Scientists (A), No. 23685034], KAKENHI, Grant-in-Aid for Scientific Research (B), No. 26289345, Fund for the Promotion of Joint International Research (Fostering Joint International Research) No. 15KK0221, Grant-in-Aid for Challenging Research (Exploratory), No. 17K19002] and Leading Research Organizations (RCUK [through EPSRC EP/I018301/1], ANR [13-G8ME-0003]) under the G8 Research Councils Initiative for Multi-lateral Research Funding—G8-2012. The authors thank the Science and Technology Facilities Council for allocation of beam time, travel and consumables (experiment number RB1710004, DOI: <https://doi.org/10.5286/ISIS.E.86389268>). This work benefited from the use of the SasView application, originally developed under NSF Award DMR-0520547. SasView also contains code developed with funding from the EU Horizon 2020 programme under the SINE2020 project Grant No 654000.

Appendix A. Supplementary data

Supplementary material related to this article can be found, in the online version, at doi:<https://doi.org/10.1016/j.carbpol.2019.115376>.

References

- Adamczyk, Z., Para, G., & Warszyński, P. (1999). Influence of ionic strength on surface tension of cetyltrimethylammonium bromide. *Langmuir*, 15, 8383–8387.
- Aswal, V. K., & Goyal, P. S. (1998). Mixed micelles of alkyltrimethylammonium halides a small-angle neutron-scattering study. *Physica B: Condensed Matter*, 245, 73–80.
- Bandyopadhyay, S., Shelley, J. C., Tarek, M., Moore, P. B., & Klein, M. L. (1998). Surfactant aggregation at a hydrophobic surface. *The Journal of Physical Chemistry B*, 102, 6318–6322.
- Bergström, M., & Pedersen, J. S. (1998). Small-angle neutron scattering (SANS) study of aggregates formed from aqueous mixtures of sodium dodecyl sulfate (SDS) and dodecyltrimethylammonium bromide (DTAB). *Langmuir*, 14, 3754–3761.
- Bergström, M., & Pedersen, J. S. (1999). Structure of pure SDS and DTAB micelles in brine determined by small-angle neutron scattering (SANS). *Physical Chemistry Chemical Physics*, 1, 4437–4446.
- Berr, S. S. (1987). Solvent isotope effects on alkyltrimethylammonium bromide micelles as a function of alkyl chain length. *The Journal of Physical Chemistry*, 91, 4760–4765.
- Biswas, S. C., & Chatteraj, D. K. (1997). Polysaccharide-surfactant interaction. 1. Adsorption of cationic surfactants at the cellulose-water interface. *Langmuir*, 13, 4505–4511.
- Brown, P., Bushmelev, A., Butts, C. P., Cheng, J., Eastoe, J., Grillo, I., et al. (2012). Magnetic control over liquid surface properties with responsive surfactants. *Angewandte Chemie International Edition*, 124, 2464–2466.
- Chua, C. K., & Pumera, M. (2013). Reduction of graphene oxide with substituted borohydrides. *Journal of Materials Chemistry A*, 1, 1892–1898.
- Coleman, J. N. (2009). Liquid-phase exfoliation of nanotubes and graphene. *Advanced Functional Materials*, 19, 3680–3695.
- Ducker, W. A., & Grant, L. M. (1996). Effect of substrate hydrophobicity on surfactant surface-aggregate geometry. *The Journal of Physical Chemistry*, 100, 11507–11511.
- Feigin, L. A., & Svergun, D. I. (1987). *Structure analysis by small-angle X-ray and neutron scattering* (1st ed). New York: Springer Chapter 1.
- Feng, Y., Zhang, X., Shen, Y., Yoshino, K., & Feng, W. (2012). A mechanically strong, flexible and conductive film based on bacterial cellulose/graphene nanocomposite. *Carbohydrate Polymers*, 87, 644–649.
- Ferrari, A. C. (2007). Raman spectroscopy of graphene and graphite: Disorder, electron-phonon coupling, doping and nonadiabatic effects. *Solid State Communications*, 143, 47–57.
- Fiscaro, E., Biemmi, M., Compari, C., Duce, E., & Peroni, M. (2007). Thermodynamics of aqueous solutions of dodecyltrimethylammonium bromide. *Journal of Colloid and Interface Science*, 305, 301–307.
- Georgakilas, V., Otyepka, M., Bourlinois, A. B., Chandra, V., Kim, N., Kemp, K. C., et al.

- (2012). Functionalization of graphene: Covalent and non-covalent approaches, derivatives and applications. *Chemical Reviews*, 112, 6156–6214.
- Granite, M., Radulescu, A., & Cohen, Y. (2012). Small-angle neutron scattering from aqueous dispersions of single-walled carbon nanotubes with Pluronic F127 and poly(vinylpyrrolidone). *Langmuir*, 28, 11025–11031.
- Griffith, A., & Notley, S. M. (2012). pH dependent stability of aqueous suspensions of graphene with adsorbed weakly ionisable cationic polyelectrolyte. *Journal of Colloid and Interface Science*, 369, 210–215.
- Hayter, J. B., & Penfold, J. (1983). Determination of micelle structure and charge by neutron small-angle scattering. *Colloid and Polymer Science*, 261, 1022–1030.
- Hollamby, M. J. (2013). Practical applications of small-angle neutron scattering. *Physical Chemistry Chemical Physics*, 15, 10566–10579.
- Hou, M., Xu, M., & Li, B. (2018). Enhanced electrical conductivity of cellulose nanofiber/graphene composite paper with a sandwich structure. *ACS Sustainable Chemistry & Engineering*, 6, 2983–2990.
- Hunter, R. J. (1981). *Zeta potential in colloid science: Principles and applications* (1st ed.). London: Academic Press Chapter 2.
- Kaniyoor, A., & Ramaprabhu, S. (2012). A Raman spectroscopic investigation of graphite oxide derived graphene. *AIP Advances*, 2, 032183.
- Karukstis, K. K., Suljak, S. W., Waller, P. J., Whiles, J. A., & Thompson, E. H. Z. (1996). Fluorescence analysis of single and mixed micelle systems of SDS and DTAB. *The Journal of Physical Chemistry*, 100, 11125–11132.
- Kiziltas, E. E., Kiziltas, A., Rhodes, K., Emanetoglu, N. W., Blumentritt, M., & Gardner, D. J. (2016). Electrically conductive nano graphite-filled bacterial cellulose composites. *Carbohydrate Polymers*, 136, 1144–1151.
- Kudin, K. N., Ozbas, B., Schniepp, H. C., Prud'Homme, R. K., Aksay, I. A., & Car, R. (2008). Raman spectra of graphite oxide and functionalized graphene sheets. *Nano Letters*, 8, 36–41.
- Lin, S., Shih, C.-J., Sresht, V., Rajan, A. G., Strano, M. S., & Blankschtein, D. (2016). Understanding the colloidal dispersion stability of 1D and 2D materials: Perspectives from molecular simulations and theoretical modeling. *Advances in Colloid and Interface Science*, 244, 36–53.
- Lin, S., Shih, C.-J., Strano, M. S., & Blankschtein, D. (2011). Molecular insights into the surface morphology, layering structure, and aggregation kinetics of surfactant-stabilized graphene dispersions. *Journal of the American Chemical Society*, 133, 12810–12823.
- Lotya, M., Hernandez, Y., King, P. J., Smith, R. J., Nicolosi, V., Karlsson, L. S., et al. (2009). Liquid phase production of graphene by exfoliation of graphite in surfactant/water solutions. *Journal of the American Chemical Society*, 131, 3611–3620.
- Magid, L. J., Li, Z., & Butler, P. D. (2000). Flexibility of elongated sodium dodecyl sulfate micelles in aqueous sodium chloride: A small-angle neutron scattering study. *Langmuir*, 16, 10028–10036.
- Mahajan, R. K., Vohra, K. K., Kaur, N., & Aswal, V. K. (2008). Organic additives and electrolytes as cloud point modifiers in octylphenol ethoxylate solutions. *Journal of Surfactants and Detergents*, 11, 243–250.
- Manne, S., Cleveland, J. P., Gaub, H. E., Stucky, G. D., & Hansma, P. K. (1994). Direct visualization of surfactant hemimicelles by force microscopy of the electrical double layer. *Langmuir*, 10, 4409–4413.
- Mao, C., Zhu, Y., & Jiang, W. (2012). Design of electrical conductive composites: Tuning the morphology to improve the electrical properties of graphene filled immiscible polymer blends. *ACS Applied Materials & Interfaces*, 4, 5281–5286.
- Matarredona, O., Rhoads, H., Li, Z., Harwell, J. H., Balzano, L., & Resasco, D. E. (2003). Dispersion of single-walled carbon nanotubes in aqueous solutions of the anionic surfactant NaDBS. *The Journal of Physical Chemistry B*, 107, 13357–13367.
- Matos, C. F., Galembeck, F., & Zarbin, A. J. G. (2014). Multifunctional and environmentally friendly nanocomposites between natural rubber and graphene or graphene oxide. *Carbon*, 78, 469–479.
- Matsuo, Y., Niwa, T., & Sugie, Y. (1999). Preparation and characterization of cationic surfactant-intercalated graphite oxide. *Carbon*, 37, 897–901.
- McCoy, T. M., de Campo, L., Sokolova, A. V., Grillo, I., Izgorodina, E. I., & Tabor, R. F. (2018). Bulk properties of aqueous graphene oxide and reduced graphene oxide with surfactants and polymers: Adsorption and stability. *Physical Chemistry Chemical Physics*, 20, 16801–16816.
- Mohamed, A., Ardyani, T., Abu Bakar, S., Brown, P., Hollamby, M., Sagisaka, M., et al. (2016). Graphene-philic surfactants for nanocomposites in latex technology. *Advances in Colloid and Interface Science*, 230, 54–69.
- Mohamed, A., Ardyani, T., Abu Bakar, S., Sagisaka, M., Umetsu, Y., Hamon, J. J., et al. (2018). Rational design of aromatic surfactants for graphene/natural rubber latex nanocomposites with enhanced electrical conductivity. *Journal of Colloid and Interface Science*, 516, 34–47.
- Mohamed, A., Ardyani, T., Abu Bakar, S., Sagisaka, M., Umetsu, Y., Hussin, M. R. M., et al. (2018). Preparation of conductive cellulose paper through electrochemical exfoliation of graphite: The role of anionic surfactant ionic liquids as exfoliating and stabilizing agents. *Carbohydrate Polymers*, 201, 48–59.
- Mohamed, A., Trickett, K., Chin, S. Y., Cummings, S., Sagisaka, M., Hudson, L., et al. (2010). Universal surfactant for water, oils, and CO₂. *Langmuir*, 26, 13861–13866.
- Moulik, S. P., Haque, M. E., Jana, P. K., & Das, A. R. (1996). Micellar properties of cationic surfactants in pure and mixed states. *The Journal of Physical Chemistry*, 100, 701–708.
- Nguyen Dang, L., & Seppälä, J. (2015). Electrically conductive nanocellulose/graphene composites exhibiting improved mechanical properties in high-moisture condition. *Cellulose*, 22, 1799–1812.
- Notley, S. M. (2012). Highly concentrated aqueous suspensions of graphene through ultrasonic exfoliation with continuous surfactant addition. *Langmuir*, 28, 14110–14113.
- Paria, S., Manohar, C., & Khilar, K. C. (2004). Effect of cationic surfactant on the adsorption characteristics of anionic surfactant on cellulose surface. *Colloids and Surfaces A: Physicochemical and Engineering Aspects*, 232, 139–142.
- Parvez, K., Wu, Z.-S., Li, R., Liu, X., Graf, R., Feng, X., et al. (2014). Exfoliation of graphite into graphene in aqueous solutions of inorganic salts. *Journal of the American Chemical Society*, 136, 6083–6091.
- Paul, A., Griffiths, P. C., Pettersson, E., Stilbs, P., Bales, B. L., Zana, R., et al. (2005). Nuclear magnetic resonance and small-angle neutron scattering studies of anionic surfactants with macrocounterions: Tetramethylammonium dodecyl sulfate. *The Journal of Physical Chemistry B*, 109, 15775–15779.
- Peng, H., Meng, L., Niu, L., & Lu, Q. (2012). Simultaneous reduction and surface functionalization of graphene oxide by natural cellulose with the assistance of the ionic liquid. *The Journal of Physical Chemistry C*, 116, 16294–16299.
- Quennou, N., Hashmi, S. M., Choi, H. S., Kim, J. W., & Osuji, C. O. (2016). Rheology of cellulose nanofibrils in the presence of surfactants. *Soft Matter*, 12, 157–164.
- Sa, V., & Kornev, K. G. (2011). Analysis of stability of nanotube dispersions using surface tension isotherms. *Langmuir*, 27, 13451–13460.
- Shah, K., Chiu, P., & Sinnott, S. B. (2006). Comparison of morphology and mechanical properties of surfactant aggregates at water-silica and water-graphite interfaces from molecular dynamics simulations. *Journal of Colloid and Interface Science*, 296, 342–349.
- Shih, C.-J., Lin, S., Strano, M. S., & Blankschtein, D. (2015). Understanding the stabilization of single-walled carbon nanotubes and graphene in ionic surfactant aqueous solutions: Large-scale coarse-grained molecular dynamics simulation-assisted DLVO theory. *The Journal of Physical Chemistry C*, 119, 1047–1060.
- Smith, R. J., Lotya, M., & Coleman, J. N. (2010). The importance of repulsive potential barriers for the dispersion of graphene using surfactants. *New Journal of Physics*, 12, 125008.
- Stone, M. T., Smith, P. G., da Rocha, S. R. P., Rossy, P. J., & Johnston, K. P. (2004). Low interfacial free volume of stubby surfactants stabilizes water-in-carbon dioxide microemulsions. *The Journal of Physical Chemistry B*, 108, 1962–1966.
- Suriani, A. B., Nurhafizah, M. D., Mohamed, A., Masrom, A. K., Sahajwalla, V., & Joshi, R. K. (2016). Highly conductive electrodes of graphene oxide/natural rubber latex-based electrodes by using a hyper-branched surfactant. *Materials & Design*, 99, 174–181.
- Suriani, A. B., Nurhafizah, M. D., Mohamed, A., Zainol, I., & Masrom, A. K. (2015). A facile one-step method for graphene oxide/natural rubber latex nanocomposite production for supercapacitor applications. *Materials Letters*, 161, 665–668.
- Tardy, B. L., Yokota, S., Ago, M., Xiang, W., Kondo, T., Bordes, R., et al. (2017). Nanocellulose-surfactant interactions. *Current Opinion in Colloid & Interface Science*, 29, 57–67.
- Texter, J. (2014). Graphene dispersions. *Current Opinion in Colloid & Interface Science*, 19, 163–174.
- Tkalya, E. E., Ghislandi, M., Alekseev, A., Koning, C., & Loos, J. (2010). Latex-based concept for the preparation of graphene-based polymer nanocomposites. *Journal of Materials Chemistry*, 20, 3035–3039.
- Tkalya, E. E., Ghislandi, M., de With, G., & Koning, C. E. (2012). The use of surfactants for dispersing carbon nanotubes and graphene to make conductive nanocomposites. *Current Opinion in Colloid & Interface Science*, 17, 225–232.
- Tucker, I. M., Petkov, J. T., Penfold, J., & Thomas, R. K. (2012). Interaction of the anionic surfactant SDS with a cellulose thin film and the role of electrolyte and polyelectrolyte. 2 Hydrophilic cellulose. *Langmuir*, 28, 10223–10229.
- Vadukumpully, S., Paul, J., & Valiyaveetil, S. (2009). Cationic surfactant mediated exfoliation of graphite into graphene flakes. *Carbon*, 47, 3288–3294.
- Vaisman, L., Wagner, H. D., & Marom, G. (2006). The role of surfactants in dispersion of carbon nanotubes. *Advances in Colloid and Interface Science*, 128–130, 37–46.
- Wang, F., Drzal, L. T., Qin, Y., & Huang, Z. (2015). Multifunctional graphene nanoplatelets/cellulose nanocrystals composite paper. *Composites Part B: Engineering*, 79, 521–529.
- Wang, H. (2009). Dispersing carbon nanotubes using surfactants. *Current Opinion in Colloid & Interface Science*, 14, 364–371.
- Wang, H., Zhou, W., Ho, D. L., Winey, K. I., Fischer, J. E., Glinka, C. J., et al. (2004). Dispersing single-walled carbon nanotubes with surfactants: A small angle neutron scattering study. *Nano Letters*, 4, 1789–1793.
- Wang, Q., Han, Y., Wang, Y., Qin, Y., & Guo, Z.-X. (2008). Effect of surfactant structure on the stability of carbon nanotubes in aqueous solution. *The Journal of Physical Chemistry B*, 112, 7227–7233.
- Wang, R., Bian, H., Ji, H., & Yang, R. (2018). Preparation of lignocellulose/graphene composite conductive paper. *Cellulose*, 25, 6139–6149.
- Wang, S., Yi, M., & Shen, Z. (2016). The effect of surfactants and their concentration on the liquid exfoliation of graphene. *RSC Advances*, 6, 56705–56710.
- Xhanari, K., Syverud, K., Chinga-Carrasco, G., Paso, K., & Stenius, P. (2011). Reduction of water wettability of nanofibrillated cellulose by adsorption of cationic surfactants. *Cellulose*, 18, 257–270.
- Xiong, R., Hu, K., Grant, A. M., Ma, R., Xu, W., Lu, C., et al. (2016). Ultrarobust transparent cellulose nanocrystal-graphene membranes with high electrical conductivity. *Advanced Materials*, 28, 1501–1509.
- Ye, Y.-S., Zeng, H.-X., Wu, J., Dong, L.-Y., Zhu, J.-T., Xue, Z.-G., et al. (2016). Biocompatible reduced graphene oxide sheets with superior water dispersibility stabilized by cellulose nanocrystals and their polyethylene oxide composites. *Green Chemistry*, 18, 1674–1683.
- Yurekli, K., Mitchell, C. A., & Krishnamoorti, R. (2004). Small-angle neutron scattering from surfactant-assisted aqueous dispersions of carbon nanotubes. *Journal of the American Chemical Society*, 126, 9902–9903.
- Zhang, X., Liu, X., Zheng, W., & Zhu, J. (2012). Regenerated cellulose/graphene nanocomposite films prepared in DMAc/LiCl solution. *Carbohydrate Polymers*, 88, 26–30.
- Zhou, J., & Zhang, L. (2000). Solubility of cellulose in NaOH/urea aqueous solution. *Polymer Journal*, 32, 866–870.